

Supplemental Information for:

Understanding Interactions of Organic Nitrates with the Surface and Bulk of Organic Films: Implications for Particle Growth in the Atmosphere

A. C. Vander Wall,[†] P. S. J. Lakey,[†] E. Rossich Molina,[‡] V. Perraud,[†] L. M. Wingen,[†] J. Xu,[†] D. Soulsby,^{††} R. B. Gerber,^{‡†*} M. Shiraiwa,^{†*} and B. J. Finlayson-Pitts^{†*}

[†]Department of Chemistry
University of California, Irvine
Irvine, CA 92697, USA

^{††}Department of Chemistry
University of Redlands
1200 East Colton Ave
Redlands, CA 92373, USA

[‡]Institute of Chemistry, Fritz Haber Research Center
Hebrew University of Jerusalem
Jerusalem 91904, Israel

Environmental Science: Processes and Impacts

*Corresponding authors: For experiments, bjfinlay@uci.edu; phone: (949) 824-7670; FAX: (949) 824-2420; for structure characterization, bgerber@uci.edu; for kinetic modeling, m.shiraiwa@uci.edu.

Section 1- Synthesized Hydroxynitrate Characterization

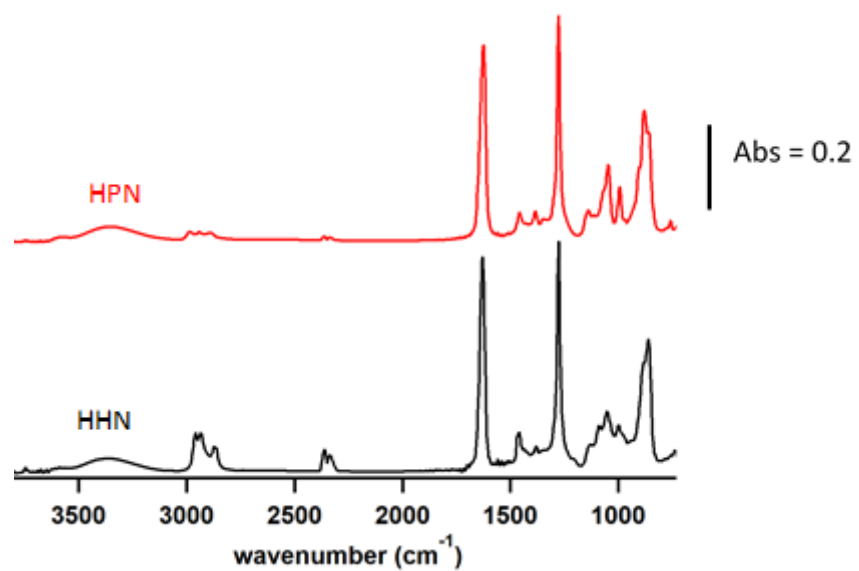


Figure S1: ATR-FTIR spectra of the pure liquid synthesized HPN (red) and HHN (black).

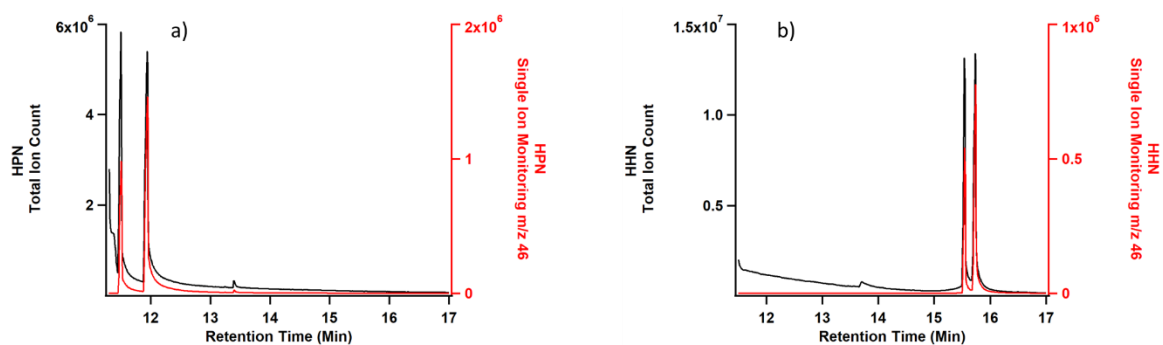


Figure S2: The GC-MS data for solutions (approximately 100 mM in dichloromethane) of a) HPN and b) HHN. Total ion chromatograms are shown in black, and single ion monitoring m/z 46 are shown in red. The two peaks indicate the two isomers (hydroxy-terminated and nitrate-terminated) present in the solution.

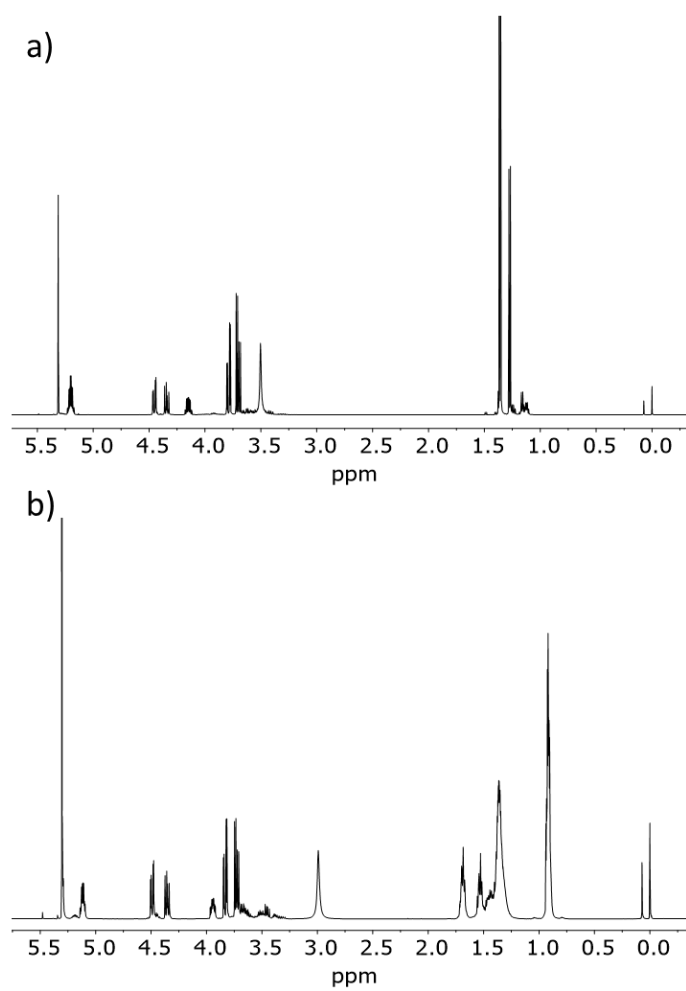


Figure S3: ^1H NMR (500 MHz, in CDCl_3 with 0.05% tetramethylsilane) of a) HPN and b) HHN.

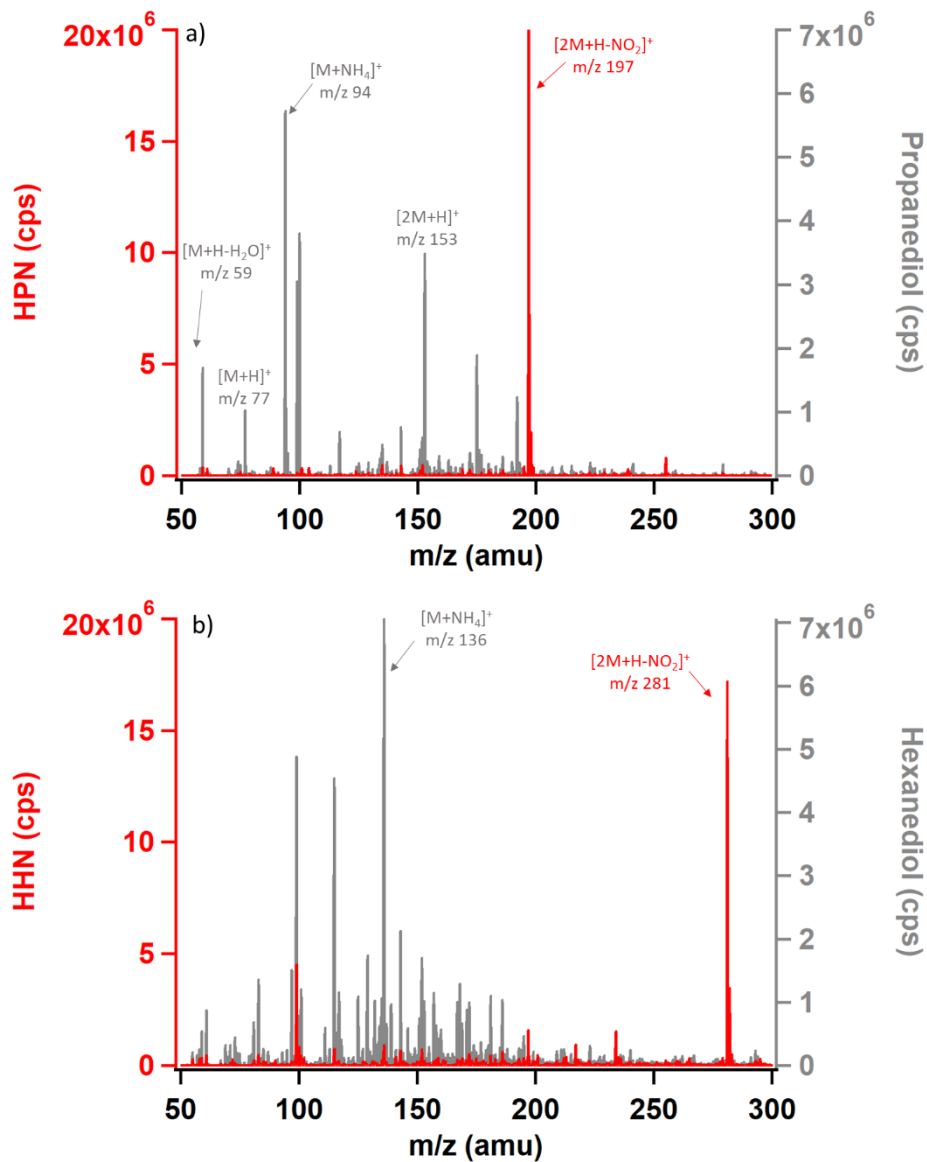


Figure S4: DART-MS spectra for the vapors from the headspace of a) pure HPN in the glass trap (red) and pure propanediol (grey), b) pure HHN in the glass trap (red) and pure hexanediol (grey).

Section 2- FTIR Absorption Cross Sections

Absorption cross sections for each organic nitrate and substrate were obtained using transmission through a 0.5 mm pathlength KBr cell or by filling the ATR cell with a solution of known concentrations ranging from 1 to 10^{-3} M, and covering the cell with a glass lid to prevent evaporation. Solutions for FTIR cross section measurements were made in either dodecane, methanol, or acetonitrile.

To calculate the pathlength within the ATR cell through a thick film such as the case when the cell is filled with solution, the effective thickness (d_e) of the solution in the cell was calculated using the wavelength of interest, and the refractive indices of the Ge crystal and the solvent.¹ Accounting for the 10 bounces within the crystal, the effective pathlength (l_{eff}) through for example an acetonitrile solution was 3.0 μm at 1730 cm^{-1} , 3.2 μm at 1630 cm^{-1} , and 4.0 μm at 1280 cm^{-1} respectively. The measured cross sections from the two methods agreed within 5% and averages are provided in Table S1, which includes the cross section at 1280 cm^{-1} for each organic nitrate, as well as the carbonyl cross section for PA, PEA and a proxy cross section for SOA comprised of the average of the cross sections of PA, tartaric acid, valeric acid and 2-nonanone.

Table S1: FTIR cross sections in $\text{cm}^2 \text{mole}^{-1} \text{-ONO}_2$ or $\text{cm}^2 \text{mole}^{-1} \text{C=O}$ (base 10) for the organic nitrates, PA, PEA, and a proxy SOA at a resolution of 8 cm^{-1} .

Compound	$\sigma^{\text{a,b}}$
	(Units of $10^5 \text{ cm}^2 \text{mole}^{-1} \text{-ONO}_2$ or $\text{mole}^{-1} \text{C=O}$, base 10)
2EHN	4.4 ± 0.1
HHN	3.2 ± 0.1
HPN	3.6 ± 0.1
PEA	3.5 ± 0.1
PA (1704 cm^{-1})	3.6 ± 0.1
Tartaric Acid	3.3 ± 0.1
Valeric Acid	1.7 ± 0.1
Nonanone	2.7 ± 0.2
SOA	2.8 ± 0.8

^aError bars are $\pm 1\sigma$.

^bCross sections were determined from the height of the characteristic peaks for each compound (1280 cm^{-1} for organic nitrates, and $1700\text{-}1730 \text{ cm}^{-1}$ for C=O) using standard solutions, and for carbonyl-containing compounds normalized to the number of carbonyls on the molecule. For PEA, six subunits of the polymer were assumed, resulting in a total of 12 C=O for every PEA molecule. Carbonyl cross section for SOA was estimated as the average of the cross sections for pinonic acid, tartaric acid, valeric acid, and nonanone.

The ATR-FTIR spectra for a solid PA film and a standard solution are shown in Figure S5. The presence of hydrogen bonding in the solid caused overlap of the acid and ketone carbonyl peaks, whereas in solution these are two distinct peaks. Due to this overlap in the solid phase, the peak cross section at 1704 cm^{-1} for the liquid solution was used to quantify the thickness of solid PA films. For all nitrates and substrates, the quantification was made based on the cross section determined from the liquid solutions.

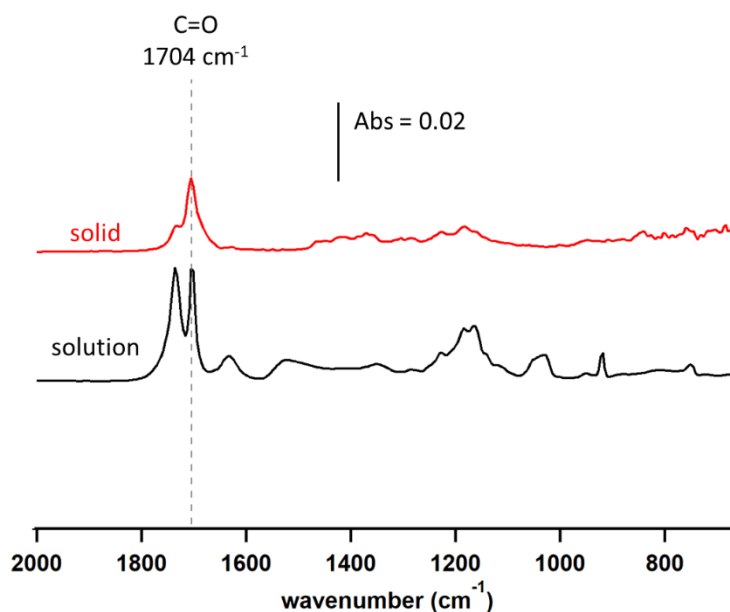


Figure S5: ATR-FTIR spectra for a solid PA film (red), and a liquid PA solution in acetonitrile (black, 56 mM). The absorbances in the black trace have been multiplied by 0.03.

The amount of organic substrate on the crystal was varied to ensure the film thickness was below the depth of penetration (d_p) of the infrared evanescent wave. The depth of

penetration was calculated from the wavelength of the peak of interest and the refractive indices of the Ge crystal and air to be $0.35\ \mu\text{m}$ at $1730\ \text{cm}^{-1}$, $0.37\ \mu\text{m}$ at $1630\ \text{cm}^{-1}$, and $0.47\ \mu\text{m}$ at $1280\ \text{cm}^{-1}$.^{1,2} For a sufficiently thin film, the path length (l) of the infrared beam through the organic film can be estimated using d_p and factoring in the 10 bounces of the beam within the ATR crystal, giving total path lengths of $3.5\ \mu\text{m}$ at $1730\ \text{cm}^{-1}$, $3.7\ \mu\text{m}$ at $1630\ \text{cm}^{-1}$, and $4.7\ \mu\text{m}$ at $1280\ \text{cm}^{-1}$.¹ The $1280\ \text{cm}^{-1}$ peak was used for analysis of the organic nitrates since there was some overlap of the substrate carbonyl peaks with the $1630\ \text{cm}^{-1}$ peak of the $-\text{ONO}_2$ group. Using both the amount of substrate deposited and the amount of nitrate taken up, partition coefficients and net uptake coefficients were quantified as described in the main text.

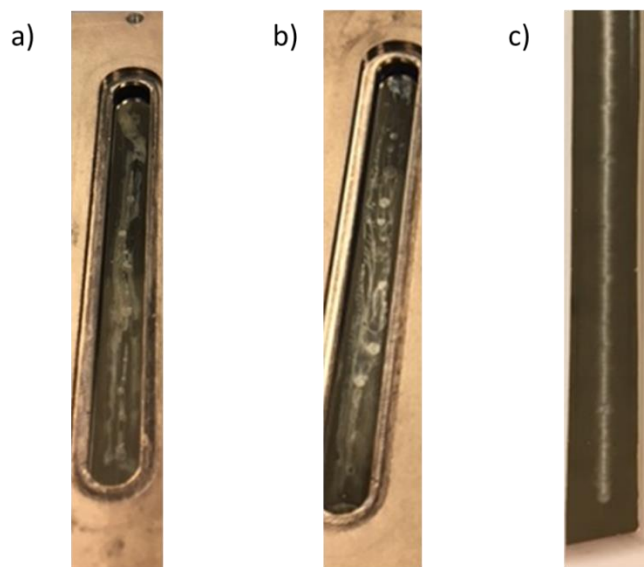


Figure S6: Typical films of a) PEA, b) PA, and c) SOA. The white regions on the crystal face show the deposited substrate scattering the overhead light.

Section 3- SOA Generation and Characterization

All reactants were introduced in the initial mixing section of the reactor.³ Gas phase α -pinene (250 ppb) was generated by injection of the pure liquid from an automated syringe pump (New Era Pump Systems Inc., Model NE-1000) into a stream of clean, dry air flowing at 10 L min⁻¹ from a purge gas generator (Parker Balston, model 75-62), carbon/alumina media (Perma Pure, LLC) and an inline 0.1 μ m filter (Headline Filters, DIF-N70). Ozone was generated by flowing 0.4 L min⁻¹ O₂ gas through a UV lamp (UVP), and subsequently was diluted with 9.6 L min⁻¹ of air before being introduced to the reactor, with resulting reactor concentrations of 250-350 ppb O₃ verified using an ozone monitor (Teledyne Photometric O₃ Analyzer – Model 400E). An additional 14 L min⁻¹ of air was introduced to create a total flow rate of 34 L min⁻¹. Experiments were performed under ambient temperature and pressure, and dry conditions (RH < 5%), without OH scavenger or seed particles.

Gas phase concentrations of α -pinene in the reactor were monitored using GC-MS with electron impact ionization (Agilent 7890A GC system with a 5975C MS detector) with the particles and ozone filtered out using a quartz filter and a KI ozone scrubber. Elemental ratios of SOA particles were measured using an aerosol mass spectrometer (Aerodyne, HR-ToF-AMS)⁴ that sampled directly from the flow reactor with a diluter in some cases. Values of O/C = 0.50 \pm 0.03 (2 σ) and H/C = 1.61 \pm 0.02 (2 σ) were determined using the method of Canagaratna *et al.*⁵

Particle size distributions were monitored using a scanning mobility particle sizer (SMPS, TSI), equipped with a model 3071A classifier and 3022A CPC, and an aerodynamic particle sizer (APS, TSI Model 3321). The size distributions were combined using the SMPS data below

500 nm and APS data above 700 nm mobility diameter assuming a particle density of 1.2 g cm^{-3} ^{3,6} and fit with a Weibull 5-parameter distribution as described by Perraud *et al.*⁷

To check the validity of the Weibull fit, an Aerodynamic Aerosol Classifier (AAC, Cambustion Ltd., UK) was used with a CPC (TSI, model 3776) to scan the entirety of the range covered by the SMPS and the APS. The AAC measures aerodynamic diameter and these diameters were converted to mobility diameters using a particle density, ρ_p , of 1.2 g cm^{-3} for pinene SOA and the Cunningham slip correction factors as a function of diameter, $C_c(d)$, as in equation (S2)⁸

$$d_a = d_m \left[\frac{C_c(d_m)}{C_c(d_a)} \right]^{1/2} \left[\frac{\rho_p}{\rho_0} \right]^{1/2} \quad (\text{S2})$$

where ρ_0 is the standard density (1.0 g cm^{-3}).

Figure S6a shows an example data set of the SMPS, APS, and Weibull fit for a representative particle number distribution, and Figure S6b shows the comparison of the Weibull fit with the AAC+CPC data for the same particle distribution. Excellent agreement is observed between the two traces, validating the Weibull fit.

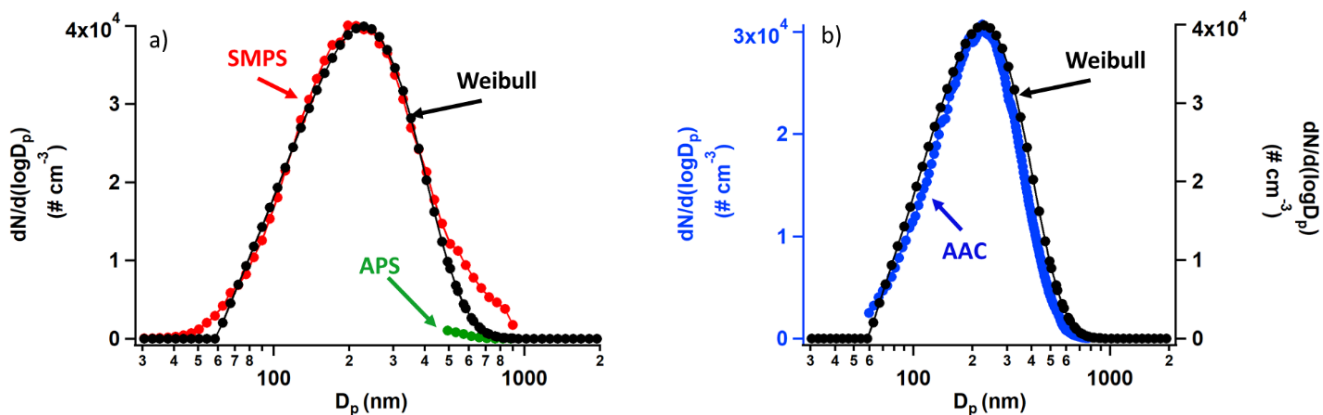


Figure S7: a) The SMPS, APS, and Weibull fit data for a representative particle number distribution, and b) the Weibull fit and AAC data for the same SOA.

Section 4- KM-GAP parameters

The bulk diffusion coefficients of the nitrate ($D_{b,nit}$) and substrate ($D_{b,sub}$) were treated to be composition-dependant using Vignes-type equations^{9, 10} as shown below:

$$D_{b,nit} = (D_{b,nit,nit})^{(1 - aF_{sub})}(D_{b,nit,sub})^{a(F_{sub})} \quad (8)$$

$$D_{b,sub} = (D_{b,sub,nit})^{(1 - F_{sub})}(D_{b,sub,sub})^{F_{sub}} \quad (9)$$

$D_{b,nit,nit}$ and $D_{b,sub,sub}$ are the diffusion coefficients of a nitrate molecule in the nitrate and a substrate molecule in the substrate, respectively, while $D_{b,nit,sub}$ and $D_{b,sub,nit}$ are the diffusion coefficients of a nitrate molecule in the substrate and a substrate molecule in the nitrate, respectively. F_{sub} is the molar fraction of the substrate in the bulk layers and a is a correction factor which takes the form of an activity coefficient. The parameter a was required in Equation 8 in order to reproduce the experimental data using a value for $D_{b,nit,nit}$ which was in the liquid range. a was assumed to be composition dependent and was parameterized using the equation shown below, which has been used successfully in previous work.^{9, 10}

$$\ln a = F_{sub}^2 (C + 3D - 4DF_{sub}) \quad (10)$$

The constants C and D as well as other parameters such as the film thickness and diffusion coefficients were determined using the Monte Carlo Genetic Algorithm (MCGA) method.¹¹ This method consists of two steps: during the Monte Carlo step, parameters are randomly varied over a range of values and a residual between the experimental data and the output is calculated.

During the genetic algorithm step, the best parameter sets are optimized using processes such as survival, recombination and mutation.

Table S2 summarizes the parameters used in the KM-GAP model that provided the best fit to the experimental data. The values of K_{nit} were fixed to values which had been determined experimentally for the specific experiments which were modeled. The value of $D_{\text{b,nit,nit}}$ was fixed to $1 \times 10^{-8} \text{ cm}^2 \text{ s}^{-1}$ for all nitrates and is a reasonable value for the self-diffusion of the nitrates, which are liquids at room temperature. Only upper limits of $D_{\text{b,sub,nit}}$ and $D_{\text{b,sub,sub}}$ are given in Table S2 as lower values had a negligible impact on the modeling results. Other input parameters in the model were the desorption lifetimes of the nitrates which were set to one μs , and the surface mass accommodations of the nitrates, which were fixed to be one.

Table S2: Input parameters used in the KM-GAP model to fit the experimental data.

Organic nitrate	Substrate	K_{nit}	$D_{\text{b,nit,nit}}$ ($\text{cm}^2 \text{s}^{-1}$)	$D_{\text{b,nit,sub}}$ ($\text{cm}^2 \text{s}^{-1}$)	$D_{\text{b,sub,nit}}$ ($\text{cm}^2 \text{s}^{-1}$)	$D_{\text{b,sub,sub}}$ ($\text{cm}^2 \text{s}^{-1}$)	C	D	Effective Initial Substrate Thickness (nm)
HHN	SOA	1.6×10^7	1.0×10^{-8}	1.4×10^{-16}	$\leq 1.0 \times 10^{-13}$	$\leq 1.0 \times 10^{-16}$	0.000	0.554	50
	PA	1.6×10^7	1.0×10^{-8}	3.7×10^{-16}	$\leq 1.0 \times 10^{-10}$	$\leq 1.0 \times 10^{-19}$	-0.072	0.421	78
	PEA	5.6×10^6	1.0×10^{-8}	2.1×10^{-19}	$\leq 1.0 \times 10^{-10}$	$\leq 1.0 \times 10^{-17}$	-0.915	0.002	119
HPN	SOA	4.9×10^5	1.0×10^{-8}	1.1×10^{-24}	$\leq 1.0 \times 10^{-14}$	$\leq 1.0 \times 10^{-16}$	-1.544	-0.498	20
	PA	1.4×10^5	1.0×10^{-8}	1.6×10^{-13}	$\leq 1.0 \times 10^{-8}$	$\leq 1.0 \times 10^{-19}$	-0.019	0.039	62
	PEA	5.1×10^4	1.0×10^{-8}	4.3×10^{-13}	$\leq 1.0 \times 10^{-8}$	$\leq 1.0 \times 10^{-17}$	-0.019	0.043	155
2EHN	SOA	1.6×10^5	1.0×10^{-8}	2.5×10^{-14}	$\leq 1.0 \times 10^{-8}$	$\leq 1.0 \times 10^{-16}$	-0.104	0.006	50
	PA	4.4×10^5	1.0×10^{-8}	1.0×10^{-15}	$\leq 1.0 \times 10^{-8}$	$\leq 1.0 \times 10^{-19}$	-0.343	0.145	36
	PEA	9.2×10^4	1.0×10^{-8}	1.4×10^{-13}	$\leq 1.0 \times 10^{-8}$	$\leq 1.0 \times 10^{-17}$	-0.006	0.223	137

Section 5- ATR-FTIR Spectra for Uptake of Organic Nitrates into Organic Substrates

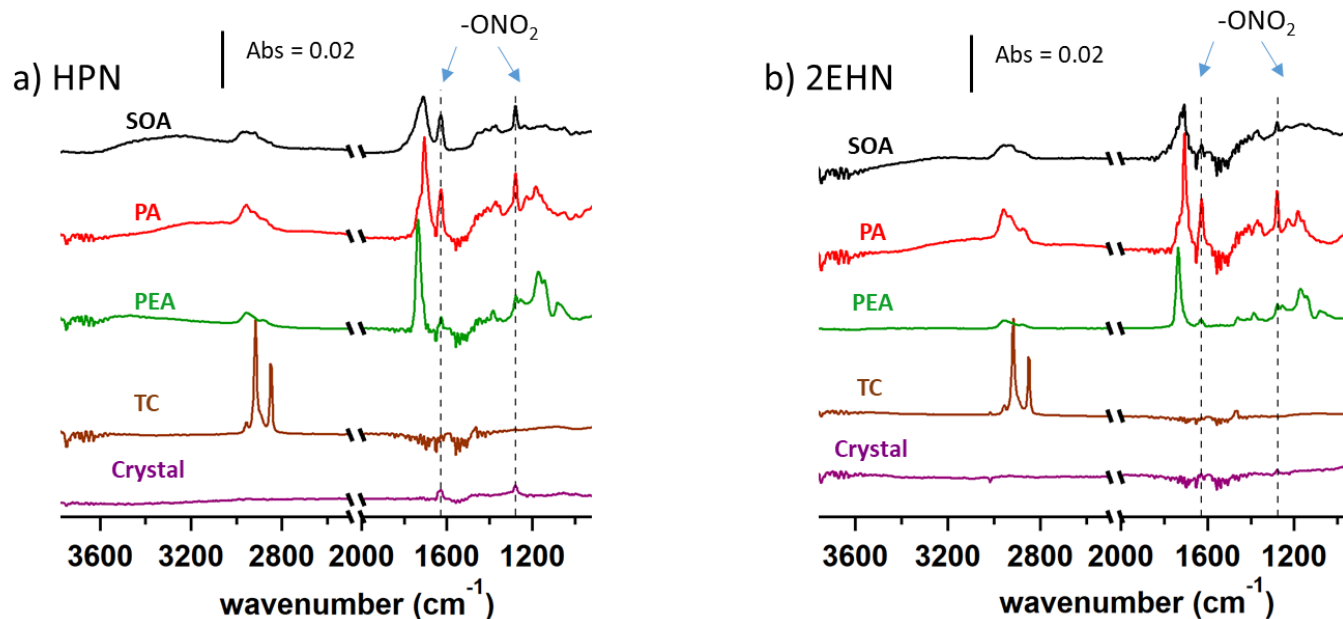


Figure S8: ATR- FTIR spectra for SOA, PA, PEA, and TC a) after exposure to gaseous HPN (250 ± 180 ppm), and b) after exposure to gaseous 2EHN (140 ppm) once equilibrium was reached (450-1050 seconds), as well as the spectra for exposure of the clean crystal to the organic nitrate. TC spectra were multiplied by a factor of 0.25, and PEA spectra by a factor of 0.5 to display them on the same scale as the other spectra for clarity. Dashed lines indicate the $-\text{ONO}_2$ signals characteristic of organic nitrates. The region between $2500\text{-}2000\text{ cm}^{-1}$ is not shown due to variations in the CO_2 (g) in the sampling compartment.

Section 6- Quantum Chemical Calculations

Table S3: Binding energies for systems of one nitrate molecule binding to one PEA subunit, and two nitrate molecules binding to one subunit for HPN, 2EHN and HHN, calculated at the B3LYP-D3/6-31+G(d) level of theory.

	Binding energy (kcal mol⁻¹)		
	HPN	2EHN	HHN
nitrate:PEA	13.5	11.8	14.5
2nitrate:PEA	18.5	18.0	30.0

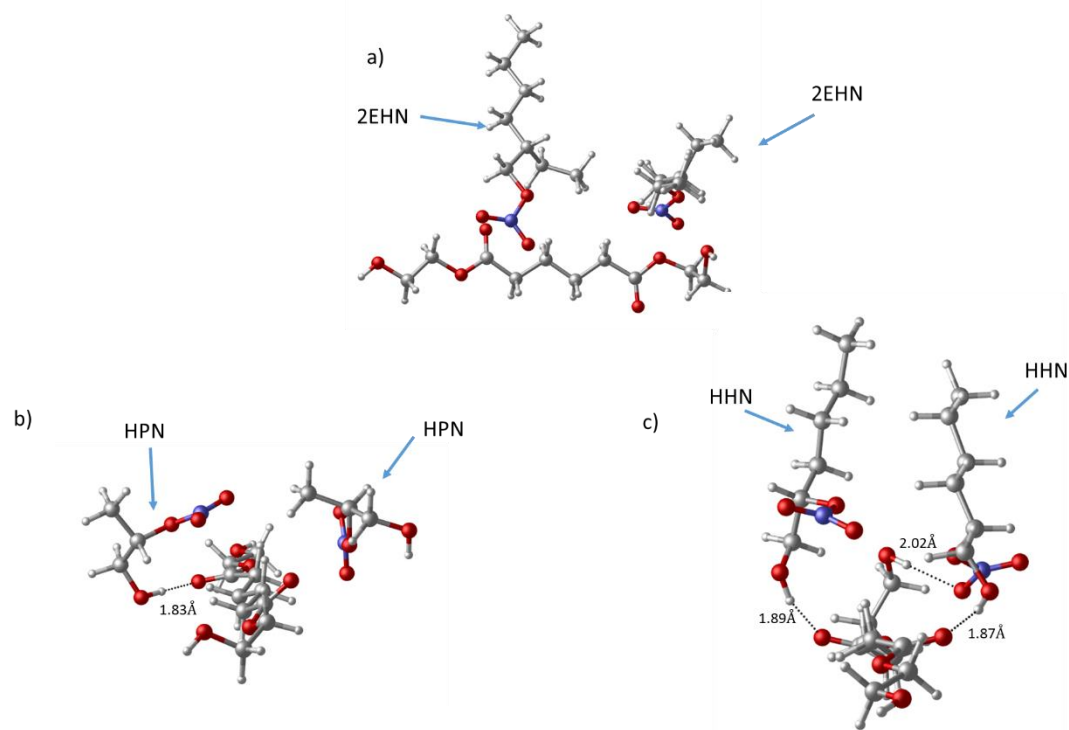


Figure S9: The optimized structures for binding of one PEA subunit to a) two 2EHN, b) two HPN, and c) two HHN. The 2EHN molecules in a) are oriented perpendicular to one another above the PEA.

Section 7- Results from KM-GAP model

Table S4: Input parameters for the KM-GAP model fit using a constant diffusion coefficient scenario.

Organic Nitrate	Substrate	K_{nit}	Effective Initial		
			Substrate Thickness (nm)	$D_{b, nit} (cm^2 s^{-1})$	$D_{b, sub} (cm^2 s^{-1})$
HHN	SOA	1.6×10^7	50	3.0×10^{-13}	$< 1.0 \times 10^{-15}$
	PA	1.6×10^7	78	6.0×10^{-13}	$< 1.0 \times 10^{-15}$
	PEA	5.6×10^6	119	7.0×10^{-13}	$< 1.0 \times 10^{-14}$
HPN	SOA	4.9×10^5	20	2.5×10^{-13}	$< 1.0 \times 10^{-14}$
	PA	1.4×10^5	62	2.0×10^{-12}	$< 1.0 \times 10^{-13}$
	PEA	5.1×10^4	155	5.0×10^{-12}	$< 1.0 \times 10^{-12}$
2EHN	SOA	1.6×10^5	50	3.0×10^{-13}	$< 1.0 \times 10^{-14}$
	PA	4.4×10^5	36	1.5×10^{-12}	$< 5.0 \times 10^{-13}$
	PEA	9.2×10^4	137	4.0×10^{-12}	$< 1.0 \times 10^{-12}$

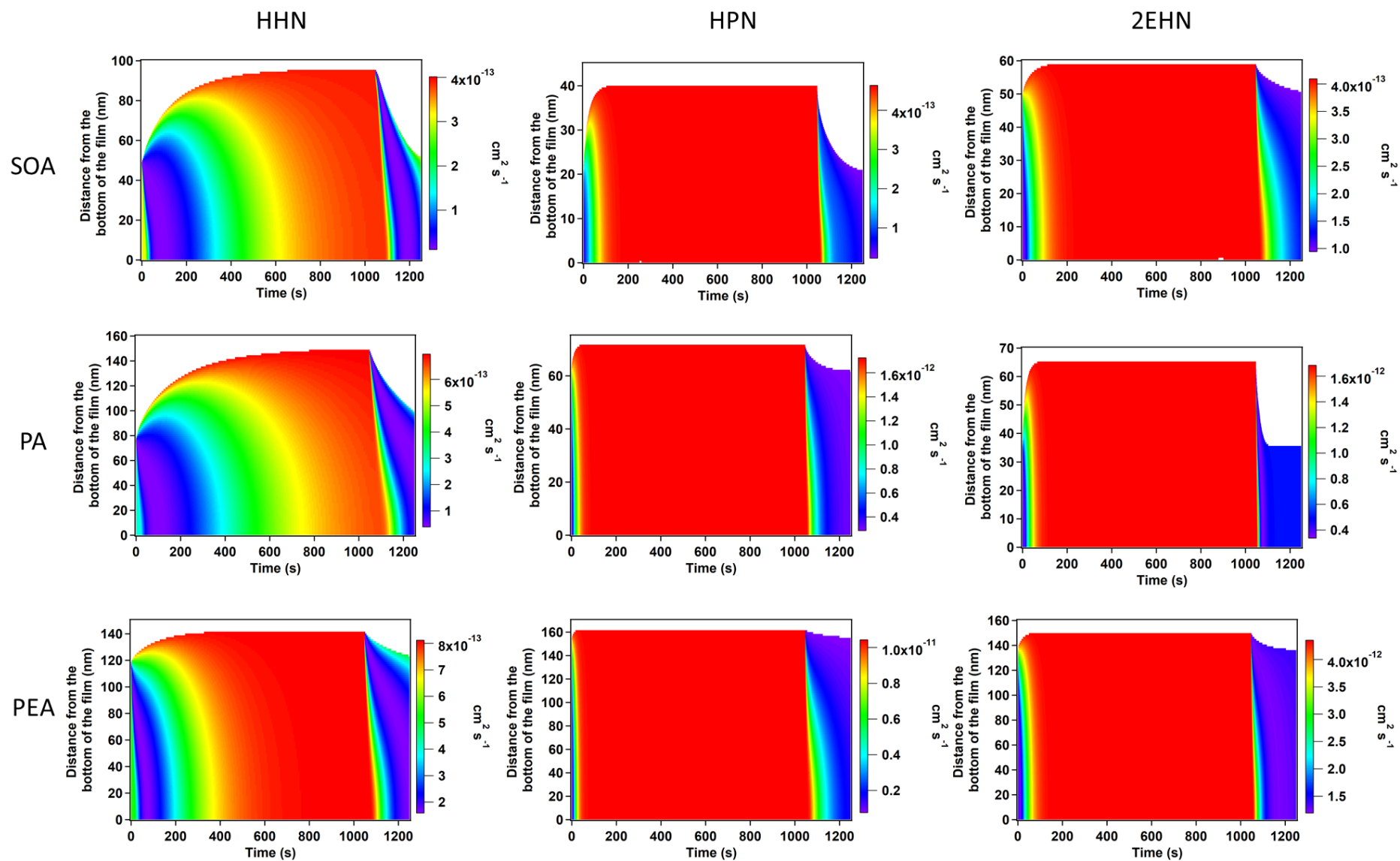


Figure S10: Contour plots showing the change in diffusion coefficient for the organic nitrate through PA, PEA, and SOA, as a function of time and distance from the bottom of the film.

References

1. N. J. Harrick, *Internal Reflection Spectroscopy*, Interscience Publishers, 1967.
2. H. Kim, B. Barkey and S. E. Paulson, Real refractive indices of α - and β -pinene and toluene secondary organic aerosols generated from ozonolysis and photo-oxidation, *J. Geophys. Res. Atmos.*, 2010, **115**, DOI: 10.1029/2010jd014549.
3. M. J. Ezell, S. N. Johnson, Y. Yu, V. Perraud, E. A. Bruns, M. L. Alexander, A. Zelenyuk, D. Dabdub and B. J. Finlayson-Pitts, A new aerosol flow system for photochemical and thermal studies of tropospheric aerosols, *Aerosol Sci. Technol.*, 2010, **44**, 329-338.
4. P. F. DeCarlo, J. R. Kimmel, A. Trimborn, M. J. Northway, J. T. Jayne, A. C. Aiken, M. Gonin, K. Fuhrer, T. Horvath, K. S. Docherty, D. R. Worsnop and J. L. Jimenez, Field-deployable, high-resolution, time-of-flight aerosol mass spectrometer, *Analytical Chemistry*, 2006, **78**, 8281-8289.
5. M. R. Canagaratna, J. L. Jimenez, J. H. Kroll, Q. Chen, S. H. Kessler, P. Massoli, L. Hildebrandt Ruiz, E. Fortner, L. R. Williams, K. R. Wilson, J. D. Surratt, N. M. Donahue, J. T. Jayne and D. R. Worsnop, Elemental ratio measurements of organic compounds using aerosol mass spectrometry: characterization, improved calibration, and implications, *Atmos. Chem. Phys.*, 2015, **15**, 253-272.
6. A. Zelenyuk, J. Yang, C. Song, R. A. Zaveri and D. Imre, A new real-time method for determining particles' sphericity and density: application to secondary organic aerosol formed by ozonolysis of α -pinene, *Environ. Sci. Technol.*, 2008, **42**, 8033-8038.
7. V. Perraud, E. A. Bruns, M. J. Ezell, S. N. Johnson, Y. Yu, M. L. Alexander, A. Zelenyuk, D. Imre, W. L. Chang, D. Dabdub, J. F. Pankow and B. J. Finlayson-Pitts, Nonequilibrium atmospheric secondary organic aerosol formation and growth, *Proc. Natl. Acad. Sci. U.S.A.*, 2012, **109**, 2836-2841.
8. W. C. Hinds, *Aerosol Technology: Properties, Behavior, and Measurement of Airborne Particles*, John Wiley & Sons, 1982.
9. D. M. Lienhard, A. J. Huisman, U. K. Krieger, Y. Rudich, C. Marcolli, B. Luo, D. L. Bones, J. P. Reid, A. T. Lambe and M. R. Canagaratna, Viscous organic aerosol particles in the upper troposphere: diffusivity-controlled water uptake and ice nucleation?, *Atmos. Chem. Phys.*, 2015, **15**, 13599-13613.
10. T. Berkemeier, S. S. Steimer, U. K. Krieger, T. Peter, U. Pöschl, M. Ammann and M. Shiraiwa, Ozone uptake on glassy, semi-solid and liquid organic matter and the role of reactive oxygen intermediates in atmospheric aerosol chemistry, *Phys. Chem. Chem. Phys.*, 2016, **18**, 12662-12674.
11. T. Berkemeier, M. Ammann, U. K. Krieger, T. Peter, P. Spichtinger, U. Pöschl, M. Shiraiwa and A. J. Huisman, Technical note: Monte Carlo genetic algorithm (MCGA) for model analysis of multiphase chemical kinetics to determine transport and reaction rate coefficients using multiple experimental data sets, *Atmos. Chem. Phys.*, 2017, **17**, 8021-8029.